Biomedical Optics EXPRESS

Effect of molecular organization on the image histograms of polarization SHG microscopy

Sotiris Psilodimitrakopoulos,[1] Ivan Amat-Roldan,[1] Pablo Loza-Alvarez,[1] and David Artigas[1,2,*]

[1]*ICFO-Institut de Ciències Fotòniques, Mediterranean Technology Park, 08860 Castelldefels (Barcelona), Spain*
[2]*Department of signal theory and communications, Universitat Politècnica de Catalunya, 08034, Spain*
**david.artigas@icfo.es*

Abstract: Based on its polarization dependency, second harmonic generation (PSHG) microscopy has been proven capable to structurally characterize molecular architectures in different biological samples. By exploiting this polarization dependency of the SHG signal in every pixel of the image, average quantitative structural information can be retrieved in the form of PSHG image histograms. In the present study we experimentally show how the PSHG image histograms can be affected by the organization of the SHG active molecules. Our experimental scenario grounds on two inherent properties of starch granules. Firstly, we take advantage of the radial organization of amylopectin molecules (the SHG source in starch) to attribute shifts of the image histograms to the existence of tilted off the plane molecules. Secondly, we use the property of starch to organize upon hydration to demonstrate that the degree of structural order at the molecular level affects the width of the PSHG image histograms. The shorter the width is the more organized the molecules in the sample are, resulting in a reliable method to measure order. The implication of this finding is crucial to the interpretation of PSHG images used for example in tissue diagnostics.

OCIS codes: (180.4315) Nonlinear microscopy; (190.2620) Harmonic generation and mixing.

References and links

1. P. Stoller, K. M. Reiser, P. M. Celliers, and A. M. Rubenchik, "Polarization-modulated second harmonic generation in collagen," Biophys. J. **82**(6), 3330–3342 (2002).
2. S. V. Plotnikov, A. C. Millard, P. J. Campagnola, and W. A. Mohler, "Characterization of the myosin-based source for second-harmonic generation from muscle sarcomeres," Biophys. J. **90**(2), 693–703 (2006).
3. F. Tiaho, G. Recher, and D. Rouède, "Estimation of helical angles of myosin and collagen by second harmonic generation imaging microscopy," Opt. Express **15**(19), 12286–12295 (2007).
4. C. Odin, T. Guilbert, A. Alkilani, O. P. Boryskina, V. Fleury, and Y. Le Grand, "Collagen and myosin characterization by orientation field second harmonic microscopy," Opt. Express **16**(20), 16151–16165 (2008).
5. S. Psilodimitrakopoulos, S. I. Santos, I. Amat-Roldan, A. K. Thayil, D. Artigas, and P. Loza-Alvarez, "In vivo, pixel-resolution mapping of thick filaments' orientation in nonfibrilar muscle using polarization-sensitive second harmonic generation microscopy," J. Biomed. Opt. **14**(1), 014001 (2009).
6. W. L. Chen, T. H. Li, P. J. Su, C. K. Chou, P. T. Fwu, S. J. Lin, D. Kim, P. T. C. So, and C. Y. Dong, "Second harmonic generation chi tensor microscopy for tissue imaging," Appl. Phys. Lett. **94**, 3 (2009).
7. V. Nucciotti, C. Stringari, L. Sacconi, F. Vanzi, L. Fusi, M. Linari, G. Piazzesi, V. Lombardi, and F. S. Pavone, "Probing myosin structural conformation in vivo by second-harmonic generation microscopy," Proc. Natl. Acad. Sci. U.S.A. **107**(17), 7763–7768 (2010).
8. P. J. Su, W. L. Chen, Y. F. Chen, and C. Y. Dong, "Determination of collagen nanostructure from second-order susceptibility tensor analysis," Biophys. J. **100**(8), 2053–2062 (2011).
9. G. Latour, I. Gusachenko, L. Kowalczuk, I. Lamarre, and M. C. Schanne-Klein, "In vivo structural imaging of the cornea by polarization-resolved second harmonic microscopy," Biomed. Opt. Express **3**(1), 1–15 (2012).
10. J. Shimada, H. Kaneko, T. Takada, S. Kitamura, and K. Kajiwara, "Conformation of amylose in aqueous solution: small-angle x-ray scattering measurements and simulations," J. Phys. Chem. B **104**(9), 2136–2147 (2000).
11. K. Beck and B. Brodsky, "Supercoiled protein motifs: the collagen triple-helix and the α-helical coiled coil," J. Struct. Biol. **122**(1-2), 17–29 (1998).

#171632 - $15.00 USD Received 29 Jun 2012; rev. 8 Sep 2012; accepted 22 Sep 2012; published 28 Sep 2012

12. S. Psilodimitrakopoulos, I. Amat-Roldan, P. Loza-Alvarez, and D. Artigas, "Estimating the helical pitch angle of amylopectin in starch using polarization second harmonic generation microscopy," J. Opt. **12**(8), 084007 (2010).
13. C. Odin, C. Heichette, D. Chretien, and Y. Le Grand, "Second harmonic microscopy of axonemes," Opt. Express **17**(11), 9235–9240 (2009).
14. S. Psilodimitrakopoulos, V. Petegnief, G. Soria, I. Amat-Roldan, D. Artigas, A. M. Planas, and P. Loza-Alvarez, "Estimation of the effective orientation of the SHG source in primary cortical neurons," Opt. Express **17**(16), 14418–14425 (2009).
15. S. Psilodimitrakopoulos, D. Artigas, G. Soria, I. Amat-Roldan, A. M. Planas, and P. Loza-Alvarez, "Quantitative discrimination between endogenous SHG sources in mammalian tissue, based on their polarization response," Opt. Express **17**(12), 10168–10176 (2009).
16. A. Erikson, J. Örtegren, T. Hompland, C. de Lange Davies, and M. Lindgren, "Quantification of the second-order nonlinear susceptibility of collagen I using a laser scanning microscope," J. Biomed. Opt. **12**(4), 044002 (2007).
17. Z.-Y. Zhuo, C.-S. Liao, C.-H. Huang, J.-Y. Yu, Y.-Y. Tzeng, W. Lo, C.-Y. Dong, H.-C. Chui, Y.-C. Huang, H.-M. Lai, and S.-W. Chu, "Second harmonic generation imaging - a new method for unraveling molecular information of starch," J. Struct. Biol. **171**(1), 88–94 (2010).
18. R. Cisek, L. Spencer, N. Prent, D. Zigmantas, G. S. Espie, and V. Barzda, "Optical microscopy in photosynthesis," Photosynth. Res. **102**(2-3), 111–141 (2009).
19. G. C. Cox, N. Moreno, and J. Feijó, "Second-harmonic imaging of plant polysaccharides," J. Biomed. Opt. **10**(2), 024013 (2005).
20. R. M. Brown, Jr., A. C. Millard, and P. J. Campagnola, "Macromolecular structure of cellulose studied by second-harmonic generation imaging microscopy," Opt. Lett. **28**(22), 2207–2209 (2003).
21. O. Nadiarnykh, R. B. Lacomb, P. J. Campagnola, and W. A. Mohler, "Coherent and incoherent SHG in fibrillar cellulose matrices," Opt. Express **15**(6), 3348–3360 (2007).
22. M. Zimmerley, R. Younger, T. Valenton, D. C. Oertel, J. L. Ward, and E. O. Potma, "Molecular orientation in dry and hydrated cellulose fibers: a coherent anti-Stokes Raman scattering microscopy study," J. Phys. Chem. B **114**(31), 10200–10208 (2010).
23. T. A. Waigh, I. Hopkinson, A. M. Donald, M. F. Butler, F. Heidelbach, and C. Riekel, "Analysis of the native structure of starch granules with x-ray microfocus diffraction," Macromolecules **30**(13), 3813–3820 (1997).
24. P.-J. Su, W.-L. Chen, J.-B. Hong, T.-H. Li, R.-J. Wu, C.-K. Chou, S.-J. Chen, C. Hu, S.-J. Lin, and C.-Y. Dong, "Discrimination of collagen in normal and pathological skin dermis through second-order susceptibility microscopy," Opt. Express **17**(13), 11161–11171 (2009).
25. J. Duboisset, D. Aït-Belkacem, M. Roche, H. Rigneault, and S. Brasselet, "Generic model of the molecular orientational distribution probed by polarization-resolved second-harmonic generation," Phys. Rev. A **85**(4), 043829 (2012).
26. Y. Chang, C. Chen, J. Chen, Y. Jin, and X. Deng, "Theoretical simulation study of linearly polarized light on microscopic second-harmonic generation in collagen type I," J. Biomed. Opt. **14**(4), 044016 (2009).
27. I. Amat-Roldan, S. Psilodimitrakopoulos, P. Loza-Alvarez, and D. Artigas, "Fast image analysis in polarization SHG microscopy," Opt. Express **18**(16), 17209–17219 (2010).
28. I. Gusachenko, G. Latour, and M.-C. Schanne-Klein, "Polarization-resolved Second Harmonic microscopy in anisotropic thick tissues," Opt. Express **18**(18), 19339–19352 (2010).
29. S. Brasselet, D. Aït-Belkacem, A. Gasecka, F. Munhoz, S. Brustlein, and S. Brasselet, "Influence of birefringence on polarization resolved nonlinear microscopy and collagen SHG structural imaging," Opt. Express **18**(14), 14859–14870 (2010).
30. P. Schön, M. Behrndt, D. Aıt-Belkacem, H. Rigneault, and S. Brasselet, "Polarization and phase pulse shaping applied to structural contrast in nonlinear microscopy imaging," Phys. Rev. A **81**(1), 013809 (2010).
31. E. Y. S. Yew and C. J. R. Sheppard, "Effects of axial field components on second harmonic generation microscopy," Opt. Express **14**(3), 1167–1174 (2006).
32. G. J. Simpson and K. L. Rowlen, "An SHG magic angle: dependence of second harmonic generation orientation measurements on the width of the orientation distribution," J. Am. Chem. Soc. **121**(11), 2635–2636 (1999).
33. M. Abdel-Akher and A. N. Michalinos, "Separation and purification of starch from chufa nut tubers *(Cyperus esculentus)*," Starch **15**(9), 329–334 (1963).
34. M. A. Swanson, "Studies on the structure of polysaccharides IV. Relation of the iodine color to the structure," J. Biol. Chem. **172**, 825–837 (1947).

1. Introduction

Up to day, developments towards the maximum acquisition of the available information in SHG imaging are based on the dependency of the produced SHG signal on the excitation linear polarization (PSHG) [1–9]. The resulting modulation in the detected SHG signal is usually fitted into a theoretical model that is taken from the nonlinear optics in crystals. This model assumes cylindrical symmetry and by analyzing the SHG modulation, the ratio of two non-vanishing, independent elements of the $\chi^{(2)}$ susceptibility tensor can be determined [2–9]. Within the molecule, the SHG response is described by the hyperpolarizability tensor $\boldsymbol{\beta}$. In

#171632 - $15.00 USD Received 29 Jun 2012; rev. 8 Sep 2012; accepted 22 Sep 2012; published 28 Sep 2012

most of the cases, a dominant orientation in $\boldsymbol{\beta}$, along an axis is also assumed. By joining the tensorial and the hyperpolarizability approaches, the SHG effective angle θ_e between the $\boldsymbol{\beta}$ axis and the long axis of the cylindrical symmetry can be estimated [2,3].

In helical molecules the helix is defined by the geometrical values given by its radius and pitch [3]. Those structural parameters have already been calculated earlier using x-ray based experiments for the several constitute molecules of starch [10], collagen [11] and muscle [11]. In SHG active molecules, the comparison of the experimentally retrieved $\boldsymbol{\beta}$ orientation with the x-ray data results in an angle θ_e that can be related to the molecule helical pitch angle [2,3,5,8]. The PSHG retrieved helical pitch angles are attributed to the polypeptide helix of the collagen triple helix [2,3,8] and to the α-helix of the myosin's tail [2,3,5] for collagen and muscle, respectively \. In plants, the helical pitch angle demonstrates amylopectin as the SHG source molecule in starch [12]. However, in no-helical molecules, such as microtubules, the angle θ_e has been associated to the geometric characteristics of the tubulin heterodimers forming the microtubule [13,14].

A recent improvement in PSHG was the presentation of the generalized bi-dimensional theoretical model which allowed the pixel by pixel fitting of the PSHG images [4,5]. It follows the introduction of the image histograms, or pixel values distributions, of the several free parameters of the biophysical model [5,6]. This results in a new source of information that can be characterized by: i) the peak or maximum frequency and ii) the width or standard deviation of the pixels' histograms [5,6]. The main idea about using these two parameters is to define metrics that allow for a proper quantification of the structural information of the sample. For example, these two parameters were used to define the conditions needed to demonstrate quantitative pixel resolution discrimination of collagen and muscle in the same image [6,15]. Thus, the different SHG sources provide different polarization modulations, providing new contrast mechanism capable to distinguish collagen, muscle and microtubules, which can be found together in the same image.

All the above PSHG studies [1–8,14,15] were performed using a bi-dimensional model which assumes that the main symmetry axis of the molecule were contained in a plane transversal to the laser excitation beam. In the present work we aim to experimentally study the effect of the existence of molecules tilted off this plane. Specifically, we focus on the interpretation of the histograms obtained for the resulting PSHG retrieved parameters. For that we use a biophysical model that considers the existence of molecules oriented off this plane [16,17]. In addition we chose starch as a sample model. Plant polysaccharides such as starch and cellulose have been imaged in the past using SHG [17–22]. Starch possesses a convenient radial structure, which allows evaluating the molecule off-plane angle. In addition, it can be found in an organized (hydrated) and disorganized (dry) form [23], which allows us to explore the use of the PSHG image histograms as a measure of the molecular organization.

Our results measuring the PSHG signal at different planes of a starch granule show how the peak of the histogram changes accordingly to the increase of molecules oriented out of the plane. This result demonstrates that a shift of the peak in the PSHG image histogram can be related to off-plane molecular orientations and not to a change in the amylopectin helical pitch. By hydrating starch, i.e., increasing the organization, we show that the PSHG image histogram becomes narrower. This indicates that the histogram width gives a measure of the structural degree of organization. Some recent applications of histogram metrics (peak position and width) have been proposed as a method to quantify structural information in diagnosis [24]. In this sense, our results are remarkable since they provide new prospects into the interpretation of the PSHG image histograms.

#171632 - $15.00 USD Received 29 Jun 2012; rev. 8 Sep 2012; accepted 22 Sep 2012; published 28 Sep 2012

2 Material and methods

2.1. Starch sample

Starch is one of the major constituents of our everyday diet and it forms granules. Starch granules are among the brightest nature-made second harmonic generation (SHG) converters [18,19]. They are basically consisting of amylose and amylopectin molecules [10,23]. The SHG source in starch has been proven to be amylopectin [12,17] and not amylose. The amylopectin molecules are oriented radially with their non-reducing chain ends pointing towards the outer surface of the granule. The radius (R) and pitch (P) of the amylopectin helix has been found using x-ray diffraction and numerical simulations modeling, resulting in 2.75 Å and 21.42 Å, respectively [10]. This results in a helical pitch angle [23] of 38.89°. Under hydration, the amylopectin molecules are further organized in a structure called crystalline lamellae [23]. In the present study we use this organization property of starch to perform comparative PSHG imaging between dried and hydrated Sigma-Aldrich (S5127, unmodified) wheat starch granules. Hydration of starch was performed using distilled water, which was added between the two 80-115 μm thickness cover slips containing the starch granule.

2.2. PSHG microscope

The setup has been described in earlier works [5,12,14,15]. It is based on an adapted inverted microscope (TE2000-U, Nikon, Japan) and a pair of galvanometric mirrors (galvos) (Cambridge Technology, UK). For the excitation source, we used a Ti:sapphire laser (MIRA 900f, Coherent, France), that was operated at a central wavelength of 810 nm. After the galvos-mirrors, we placed a linear polarizer (ThorLabs, LPNIR050, USA) parallel to the incoming linear polarization of the laser source. This was followed by a zero order λ/2 wave plate (QWPO-810, CVI Melles Griot) on a motorized rotational stage (AG-PR100, Newport Corporation), which was rotated in steps to change the polarization at the sample plane. A telescope arrangement was used to ensure that a collimated beam was filling the back aperture of the objective lens. The two excitation objectives used throughout our experiments were the 60x [(NA) = 1.4, PlanApo, Nikon, Japan] and the 40x [(NA) = 0.6, PlanApo, Nikon, Japan]. For the collection of the signals we used an identical 60x [(NA) = 1.4, Nikon, Japan] and a 40x [(NA) = 0.95, PlanApo, Nikon, Japan]. In the forward collection geometry a proper mount and detection unit was implemented. This unit could mount the collecting objective, a long-wave-pass dichroic beam splitter (FF665, Semrock Inc), a BG39 filter, a 15 nm FWHM band pass filter centered at 406 nm (FF01-406/15-25, Semrock Inc) and a PMT (H9305-04, Hamamatsu, France). A labVIEW interface program was written to control the raster scanning of the galvo-mirrors and the data acquisition (DAQ) card. Typical frame acquisition times for a single 500 x 500 pixels image were about 1-2*s*. Any effect on the depolarization of the fundamental beam introduced by the different optical components was assessed at the sample plane, by measuring the extinction ratio of the fundamental incident light for every polarization. The polarization of the laser source has a typical extinction ratio value of >500:1. The average extinction ratios for all the used (nine) polarizations were 63 ± 3:1 after the dichroic mirror and 25 ± 2:1 after the 1.4NA objective. The differences in power for each polarization were lower than 5%.

2.3. PSHG intensity from an arbitrary 3D-oriented molecule with cylindrical symmetry

Several biophysical models for interpreting the PSHG contrast have been proposed in the past [2–9,25]. Here, we are based on the model described in Ref. [5,16,17] to provide a pixel-by-pixel analysis without relying on the use of polarization analysis in detection or any sample alignment or rotation. Specifically, based on the helical nature of the amylopectin molecule, and similarly to other helical molecules, we assumed cylindrical symmetry (analytical deduction and justification of the assumed cylindrical symmetry model is depicted in the Appendix of Ref. [26]). Under Kleinman's and cylindrical symmetry conditions the $\chi^{(2)}$ tensor

#171632 - $15.00 USD Received 29 Jun 2012; rev. 8 Sep 2012; accepted 22 Sep 2012; published 28 Sep 2012

contains only 7 nonzero elements, in particular two of them are independent: $d_{15} = d_{xxz} = d_{xzx} = d_{24} = d_{yyz} = d_{yzy} = d_{32} = d_{zyy} = d_{31} = d_{zxx}$ and $d_{33} = d_{zzz}$ However, at this point we allow $d_{15} \neq d_{31}$ to experimentally check the validity of the above assumed symmetry conditions. As we define the laboratory coordinates system *X*-*Y*-*Z*, the laser is propagating along the laboratory *Z*-axis and its linear polarization is rotating in the *X*-*Y* plane at an angle α with respect to the *X*-axis. Then the electric field can be written in terms of the lab coordinates as (Fig. 1(a))

$$\vec{E} = E_0(\cos\alpha\hat{X} + \sin\alpha\hat{Y})\exp[kZ - \omega t]. \tag{1}$$

The $\chi^{(2)}$ tensor coordinates are chosen in such a way that the *y*-axis is contained in the *X*-*Y* plane and the *z*-axis coincides with the principal axis of the cylindrical symmetry (Fig. 1(b)). With this geometry, the relation between the lab and the $\chi^{(2)}$ tensor frames is given by two angles, δ and ϕ, resulting in the following change of base:

$$\begin{cases} \hat{X} = \cos\delta\cos\phi\hat{x} - \sin\phi\hat{y} + \sin\delta\cos\phi\hat{z} \\ \hat{Y} = \cos\delta\sin\phi\hat{x} + \cos\phi\hat{y} + \sin\delta\sin\phi\hat{z} \\ \hat{Z} = -\sin\delta\hat{x} + \cos\delta\hat{z} \end{cases} \tag{2}$$

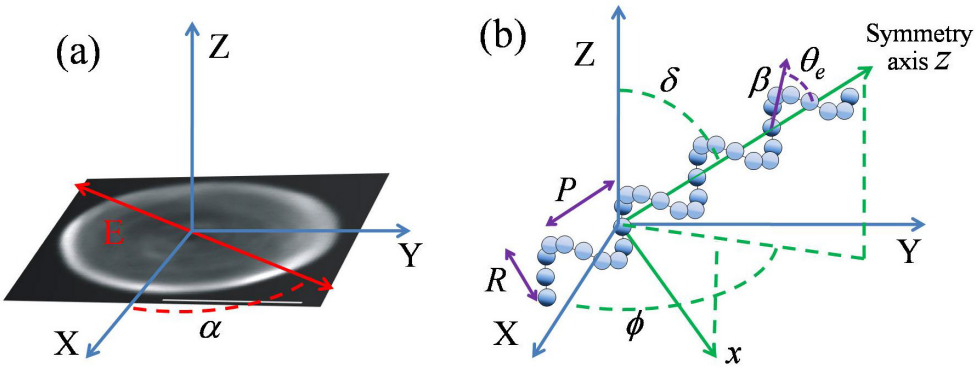

Fig. 1. Coordinates system of the 3D PSHG biophysical model. (a) SHG image of starch with the lab coordinate system (blue axis) and polarization orientation for the incident electric field (red). (b) Tensor (molecule) coordinate system (green axis). In purple, radius *R* and pitch *P*, helical pitch angle θ_e and hyperpolarizability β. The dimensions of the figure are nominal and do not correspond to reality.

Then, the amplitude in Eq. (1) transforms into

$$\vec{E} = E_0[\cos\delta\cos(\phi-\alpha)\hat{x} + \sin(\phi-\alpha)\hat{y} + \sin\delta\cos(\phi-\alpha)\hat{z}]. \tag{3}$$

From this point, taking into account the nonzero elements of the $\chi^{(2)}$ tensor, the nonlinear polarization can be expressed as

$$\Rightarrow \begin{cases} P_x^{2\omega} \sim E_0^2 2d_{15}\left\{\cos^2(\phi-\alpha)\cos\delta\sin\delta\right\} \\ P_y^{2\omega} \sim E_0^2 d_{15}\left\{\sin 2(\phi-\alpha)\sin\delta\right\} \\ P_z^{2\omega} \sim E_0^2\left\{d_{31}[\sin^2(\phi-\alpha) + \cos^2(\phi-\alpha)\cos^2\delta] + d_{33}\cos^2(\phi-\alpha)\sin^2\delta\right]\right\} \end{cases} \tag{4}$$

By using $\vec{E}_{rad}^{2\omega} = \hat{k}\times(\overrightarrow{P^{2\omega}}\times\hat{k})$, the detected average power (without analyzers) can be expressed in terms of the tensor ratio and the two angles, δ and ϕ, as

#171632 - $15.00 USD Received 29 Jun 2012; rev. 8 Sep 2012; accepted 22 Sep 2012; published 28 Sep 2012

$$I^{2\omega} \sim d_{15}^2 E_0^4 \sin^2\delta\{\sin^2 2(\phi-\alpha) + [\frac{d_{31}}{d_{15}}\sin^2(\phi-\alpha) + (\frac{d_{33}}{d_{15}}\sin^2\delta + (2+\frac{d_{31}}{d_{15}})\cos^2\delta)\cos^2(\phi-\alpha)]^2\}. \quad (5)$$

2.4. Single axis-molecule approximation

Now we are assuming dominant hyperpolarizability $\beta^{(2)}_{vvv}$ along axis-*v,* where μ,v,ξ is the hyperpolarizability coordinate system. The $\chi^{(2)}$ tensor is then described in the molecular frame using: $d_{ijk} \sim N\left\langle(\hat{i}\,\hat{v})(\hat{j}\hat{v})(\hat{k}\hat{v})\right\rangle\beta^{(2)}_{vvv}$, where N is the density of sources and $\langle\ \rangle$ denotes their orientation average. Then, assuming a random distribution of source molecules in the azimuth plane, the components of the $\chi^{(2)}$ tensor can be expressed as $d_{33} = N\left\langle\cos^3\theta\right\rangle\beta^{(2)}_{vvv}$, and $d_{15} = d_{31} = N\left\langle\cos\theta\sin^2\theta\right\rangle\beta^{(2)}_{vvv}/2$ [2,3]. If in addition a highly picked distribution of effective angles inside each pixel is assumed, the operator $\langle\ \rangle$ can be removed, yielding [3]

$$\frac{d_{33}}{d_{15}} = \frac{2}{\tan^2\theta_e}, \quad (6)$$

where θ_e, is the PSHG experimentally retrieved effective orientation or helical pitch angle of the SHG source molecule. The angle θ_e is now correlated to the pitch angle of a single helix. A single helix is described by its radius R and its pitch, P (Fig. 1(b)) and the helical pitch angle θ_e is extracted using [3]

$$\tan\theta_e = \frac{2\pi R}{P}. \quad (7)$$

2.5. Fitting procedure

In order to obtain structural information in every pixel, Eq. (5) is rewritten as

$$I^{2\omega} \sim E\left\{\sin^2 2(\alpha-\phi) + [A\sin^2(\alpha-\phi) + B\cos^2(\alpha-\phi)]^2\right\}, \quad (8)$$

where

$$E = d_{15}^2 E_0^4 \sin^2\delta, \quad (9)$$

$$A = d_{31}/d_{15}, \quad (10)$$

$$B = \frac{d_{33}}{d_{15}}\sin^2\delta + \left(2+\frac{d_{31}}{d_{15}}\right)\cos^2\delta. \quad (11)$$

The parameters, E, A, B and ϕ are the free parameters to be retrieved. In our experiments the incoming linear polarization was rotated between 0°-160°, in steps of 20°. This results in 9 images, one for every polarization. This value is considered adequate to experimentally retrieve the 4 free parameters of Eq. (8) [5]. Then, the 9 images were fed into an algorithm based on a nonlinear least-squares fitting routine (The Mathworks, Champaign-Urbana, IL). For that we used four hundred iterations to fit in every pixel the PSHG modulation to Eq. (8). Alternatively, a fast Fourier-based algorithm can be used to retrieve the free parameters [27], resulting in similar results. We have realized that there is an intrinsic indetermination. This occurs because, the values of A and B can be interchanged only by changing ϕ to $\phi + \pi/2$, giving the same result. In order to solve this, we have imposed that the larger of the two coefficients given by the fitting algorithm always is assigned to B, adding a phase $\pi/2$ to angle ϕ when the interchange is required.

#171632 - $15.00 USD Received 29 Jun 2012; rev. 8 Sep 2012; accepted 22 Sep 2012; published 28 Sep 2012

Once A, B are retrieved, the angle δ giving the molecule tilted off the focal plane can be obtained from Eqs. (10) and (11) as

$$\sin^2\delta = \frac{B - A - 2}{\frac{d_{33}}{d_{15}} - A - 2}, \tag{12}$$

where d_{33}/d_{15} can be obtained from Eq. (6) and the literature using Eq. (7).

3. Results and discussion

3.1. Considerations on the biophysical model

Experimental errors due to depolarization, axial components introduced by high numerical aperture objectives, detector saturation, sample birefringence, scattering, aberrations, etc., can greatly affect PSHG measurements [28–31]. Ideally, a biophysical model should take these effects into account. However, their pixel-by-pixel identification in PSHG imaging of biological samples requires the use of extra optical components, such as analyzers. However, it is a usual election to use the biophysical model described here, that due to the simplicity of the required set-up, is more suitable for imaging. We also propose the use of the determination coefficient r^2 of the fitting algorithm. This coefficient, besides quantifying the fitting procedure, can be used to remove the erroneous information. Equation (8) provides the different parameters E, A, B and ϕ in every pixel. In the case of important depolarization, birefringence or detection saturation, the PSHG response does not follow Eq. (8) resulting in a low r^2. By thresholding pixels with low r^2, most of the pixels affected by the previous effects can be removed from the image, as described in Ref. [5]. Then, by plotting the PSHG image histogram (for a certain region of interest (ROI)), reliable metrics can be obtained, allowing for the regions' structure quantification (i.e. by measuring the maximum, the mean, the width, the median, etc. [5,6,8,12,14,15,24]).

To start with the analysis of our simplified model, we look at the amplitude parameter, E which is related to the total generated SHG signal. From Eq. (9) we can see that the amplitude depends on the excitation field amplitude E_0 and the tensor coefficient d_{15}. However, the only readily information that can be extracted from this equation is that, molecules oriented perpendicular to the plane ($\delta = 0°$) do not contribute to the SHG signal, as can be seen in the center of the granule in Fig. 2(a).

In the case of the retrieved symmetry parameter A, it is possible to see, from Eq. (10), that any change on its image histogram should be due to a change in the tensor ratio d_{31}/d_{15}. Here, if cylindrical and Kleinmans' symmetry conditions are assumed to be valid, the retrieved value for A should be a δ-Dirac function at $d_{31}/d_{15} = 1$. That means that any deviation from this value, should be attributed to departure from Kleinmans' symmetry conditions.

This is different for the parameter B, also called the anisotropy parameter. Equation (11) indicates that together with experimental errors, there are two additional possible causes of a variation in the image histogram of B, namely, changes in the tensor ratio d_{33}/d_{15} and in the angle δ. A change in the tensor ratio d_{33}/d_{15} can be associated, through Eq. (6), to a change at the supramolecule itself, while the angle δ is the off-plane orientation of the molecules. If $\delta = 90°$, in Eq. (11) $B = d_{33}/d_{15}$, and we obtain the standard equation, or the 2D approach, of the biophysical model, used in previous studies [3,5,6,-8,12-15,24,26,31]:

$$I^{2\omega} \sim d_{15}^2 E_0^4 \left\{ \sin^2 2(\alpha - \phi) + \left[\frac{d_{31}}{d_{15}} \sin^2(\alpha - \phi) + \frac{d_{33}}{d_{15}} \cos^2(\alpha - \phi) \right]^2 \right\}, \tag{13}$$

It is interesting to note that from the point of view of the retrieving algorithm, both the 2D and the 3D models (Eq. (13) and (5), respectively) reduce to Eq. (8). This means that our retrieving procedure is blind to the use of the 2D or the 3D approaches. Then, the meaning of

#171632 - $15.00 USD Received 29 Jun 2012; rev. 8 Sep 2012; accepted 22 Sep 2012; published 28 Sep 2012

B must be sought in Eq. (11). When working with a 2D model, $B = d_{33}/d_{15}$, any variation from pixel to pixel in the value of B is attributed to a variation on the tensor ratio d_{33}/d_{15} and in the helical pitch (through Eq. (6)). Therefore, the 2D model is intrinsically attributing a change at the molecular level (helical pitch angle) as origin of the variation in B. In contrast, when the 3D model is used, i.e., B is defined by Eq. (11), any variation from pixel to pixel can be either attributed to a variation on the tensor ratio d_{33}/d_{15} or to the existence of molecules oriented off-plane ($\delta \neq 90°$). In those situations (like in a starch granule) where the molecular orientation is expected to change from pixel to pixel, the second approach is more likely to describe the variation in B.

Finally, we note that the angle δ in Eq. (12) is not defined for $B = 3$ if simultaneously Kleinmans' symmetry ($A = d_{31}/d_{15} = 1$) is assumed. Using this value ($B = 3$) in Eq. (6) we find an effective orientation or helical pitch angle of the SHG source molecule of $\theta_e = 39.23°$. This value coincides with the so called "the magic angle" defined in Ref. [32]. This angle value is obtained when Eq. (6) diverges due to maximum disorganization within one pixel.

3.2. Equatorial 3D-PSHG of hydrated wheat granules

To experimentally prove the concept outlined above, we use starch as a model sample. Rotation of the linear polarization reaching the granule resulted in a $\sin^2$ SHG intensity dependence, a behavior characteristic of a radial structure (data not shown). The radial architecture of amylopectin in our starch samples has been previously demonstrated using PSHG [12] and it is consistent with other experimental techniques [23]. That makes starch a convenient sample to analyze the effect of molecules tilted off the focal plane.

Firstly we performed PSHG imaging close to the equator of a hydrated granule. The equator is assumed to be located at the position where we recorded the maximum SHG signal. In Fig. 2 we present the images created after the pixel by pixel analysis of a hydrated starch granule for the SHG intensity and the parameters ϕ, A, B, θ_e and angle δ. To reduce the impact

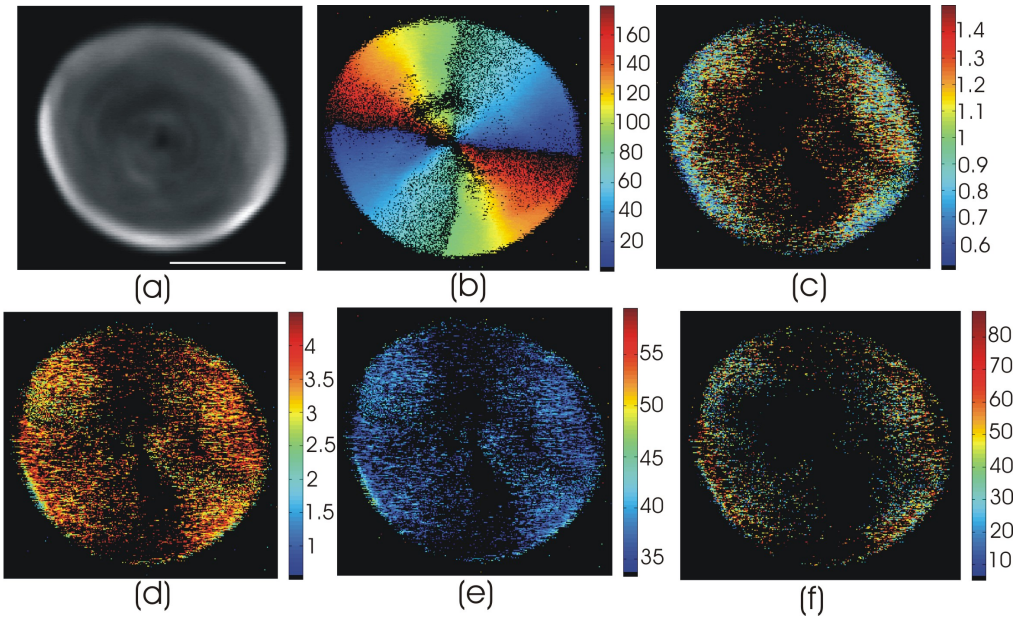

Fig. 2. 3D-PSHG in hydrated starch (a) mean intensity of the 9 PSHG images. Scale bar corresponds to 10 μm. (b) Angle ϕ giving the orientation of the molecule in the focal plane. The radial architecture of amylopectin is shown in the evolution of the angle. (c) $A = d_{31}/d_{15}$ checks the validity of the model assumptions. (d) anisotropy parameter B defined by Eq. (11). (e) Pixel resolution representation of the helical pitch angle θ_e. (f) Pixel resolution representation of the tilted-off the plane angle δ.

#171632 - $15.00 USD Received 29 Jun 2012; rev. 8 Sep 2012; accepted 22 Sep 2012; published 28 Sep 2012

of possible experimental errors (i.e. signal saturation, depolarization or polarization ellipticity, among others), only those pixels which exhibited a fitting coefficient of determination (r^2) bigger than 95% were preserved in the images. Moreover, the images were filtered using $0.5<A<5$ and $0<B<10$. In this way spurious solutions without physical meaning were also removed. The previous restrictions have caused the missing pixels observed in Fig. 2(b-f).

Figure 2(b) shows the orientation ϕ of the amylopectin molecules in every pixel. This result confirms the radial symmetry of our samples. Note however that the orientation for 0° does not coincide with the horizontal direction. This shift in the determination of ϕ is caused by the optical activity of starch granules, which induces the rotation of the excitation polarization [33]. Nevertheless, it does not influence the measured polarization intensity modulation, and therefore, the retrieved parameters A and B are not affected.

We have chosen to maintain the ratio $A = d_{31}/d_{15}$ in our fitting procedure, to experimentally check whether both, Kleinman's symmetry and the cylindrical symmetry assumption hold. The value distribution of the A parameter is shown in Fig. 2(c). Taking as a region of interest the whole granule, we use the peak and the width (defined as 2σ of a normal distribution) of the histogram as a source of information. For that, the image histogram of Fig. 2(c) is shown in Fig. 3(a). The result for the peak of parameter $A\sim1$ shows that $d_{31} = d_{15}$. Therefore, the cylindrical symmetry hypothesis and the Kleinman's symmetry conditions do hold in starch. This result agrees with the absorption spectrum of starch, whose maximum is at 600 nm, with 200 nm bandwidth [34] and therefore, a negligible departure from $A = 1$ could be expected.

Figure 2(d) shows the spatial distribution of the B parameter and the corresponding histogram is shown in Fig. 3(b). The interpretation of the B parameter requires the use of the two approaches outlined in subsection 3.1. In the first approach, because of the starch's radial geometry, the amylopectin molecules close to the equator of the granule are expected to mainly lay parallel to the sample, i.e., more perpendicular to the direction of the laser propagation. Then, $\delta = 90°$ can be assumed in Eq. (11) and the helical pitch angle θ_e can be obtained using Eq. (6). The results for the θ_e spatial distribution and image histogram are

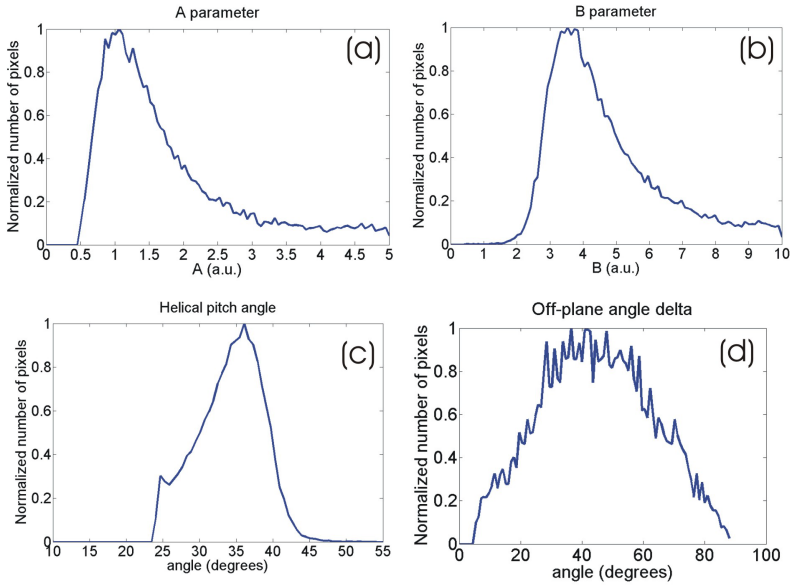

Fig. 3. Equatorial histograms of hydrated starch. (a) $A = d_{31}/d_{15}$ peak at 1.01, width of 0.50. (b) B parameter, peak at 3.54, width of 1.14. (c) Helical pitch angle θ_e retrieved from B considering the 2D approach. Peak at 36.1°, width of 4.9°. (d) Tilted-off the plane angle δ, peak at 48°, mean 44,8°, width of 36 °.

#171632 - $15.00 USD Received 29 Jun 2012; rev. 8 Sep 2012; accepted 22 Sep 2012; published 28 Sep 2012

shown in Fig. 2(e) and Fig. 3(c), respectively. The results show that the peak is close to θ_e = 36.1°, similar to the one found in Ref. [12] and to the value obtained with x-ray diffraction [3], showing the quality of the measurement. In the second approach, the tensor ratio in Eq. (12) must be fixed to find the off-plane angle δ in every pixel. Since, the experimentally retrieved helical pitch approaches the one obtained by x-ray diffraction and it is close to previous results, we chose to use this value to obtain the pixel distribution and the image histogram for the off-plane angle δ shown in Figs. 2(f) and 3(d), respectively. The resulting image histogram of δ is centered at 44.8° (mean). This indicates that the measurement is probably performed slightly out of the equator and it is in agreement with the starch's radial geometry: At the edges of the granule the molecules are mostly lying parallel to the image plane (maximum SHG signal in Fig. 2(a)), while when moving towards the center of the granule, they are gradually oriented out of the image plane until oriented almost perpendicular (minimum SHG signal in Fig. 2(a)). This behavior is in accordance with the image histogram of Fig. 3(d). These results indicate that the existence of molecules oriented off-plane is a major contribution for the width shown in the histogram distribution of the *B* parameter (Fig. 3(b)).

3.3. Effect of molecules tilted off the plane

In order to better examine the effect of molecules which are tilted off the focal plane in PSHG imaging we moved the focal plane ~5μm up from the previous position, resulting in a PSHG image of a different plane, but for the same starch granule (Fig. 4(a)). As a consequence, the distribution of amylopectins' orientation in the new image plane is different than in the previous measurement. This is an ideal situation to identify how the analysis based on image histograms is affected by molecules tilted-off the sample plane. In particular, the histogram for the parameter *A* (Fig. 4(b)), as expected from the theory, is similar in both imaging planes, showing the quality of the measurement. Figure 4(c) shows that away from the equatorial plane, the distribution of *B* values shifts to smaller values. This result can be interpreted in a different way depending on the handling of Eq. (11). On one hand, the interpretation of fixing $\delta = 90°$ in Eq. (11), leads to the determination of d_{33}/d_{15} and the calculation of the helical pitch angle using Eq. (6) (the classical approach). In this case, the shift in *B* is interpreted as an increase for the helical pitch angle (see Fig. 4(d)), and thus, this would indicate an average change at the molecular level. However, in the case of a starch granule, there is no reason to have a molecular change depending on the analyzed plane. On the other hand, as performed in

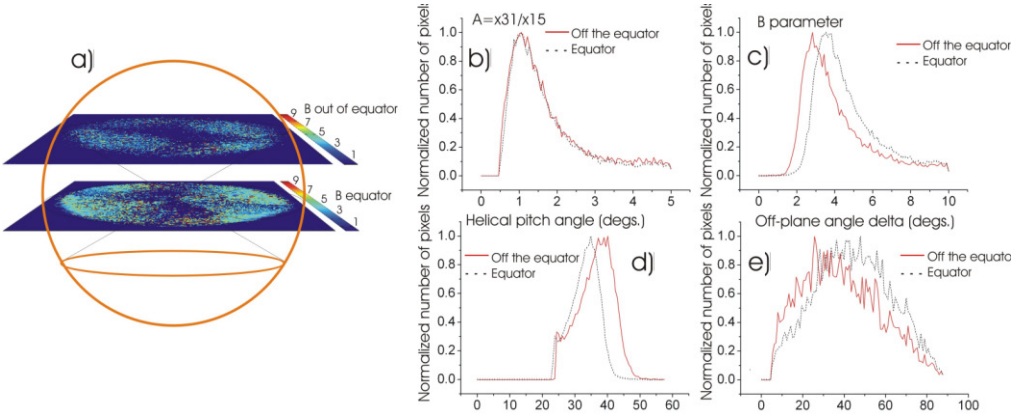

Fig. 4. (a) Schematics of the measurement preformed in the starch granule, showing the two imaged planes for the B parameter at the equator and ~5μm up from this position. Comparison of the image histograms obtained from the two measurements for (b) *A*, (b) *B*, (c) θe, and (d) δ, showing the effect of the existence of a large number of molecules tilted-off the plane: The peak shifts between the two imaged planes for *B*, θ_e and δ, but not for *A* parameter.

#171632 - $15.00 USD Received 29 Jun 2012; rev. 8 Sep 2012; accepted 22 Sep 2012; published 28 Sep 2012

the previous measurement, the tensor ratio can be fixed to the value obtained in section 3.2, i.e., d_{33}/d_{15} = 3.7. Then the image histogram distribution for the resulting angle δ presents a shift to lower values (see Fig. 4(e)). This result is consistent with the fact that off of the equator, the number of molecules oriented parallel to the sample plane (δ = 90°) decreases and as consequence a shift in the orientation towards δ = 0 is expected.

The above results show how the radial geometry affects to the results in the B parameter measured out of the equator. The effect of the radial geometry, should also be reflected when the granule is analyzed at different regions of interest (ROI) in the equator. Figure 5 shows three different ROI and the corresponding histograms for the retrieved angle δ. We can observe that in ROI 1 (at the outer part of the granule) the peak of the histogram is near 70°, showing that most of the molecules lay in the plane. However, as we move to the inner part of the granule, the peak of the histogram evolves to 45° in ROI 2 and to 30° in ROI 3, showing how the number of molecules oriented vertically increases in the center. These results are in agreement with the radial geometry and the fact that the measurement is probably performed slightly out of the equator (discussion in section 3.2 describing the histogram distribution shown in Fig. 3(d)).

All the above results are consistent with the radial geometry of starch and with the theoretical model attributing any change in B to the existence of molecules tilted off-plane and not to variations at the molecular level, i.e., a variation of the helical pitch. Finally, the PSHG analysis presented here was performed in ten granules. The statistics (average and standard deviation) for the histograms peak and width of the different retrieved parameters, both in and out of the equator, are presented in Table 1, showing the consistence of the measurements.

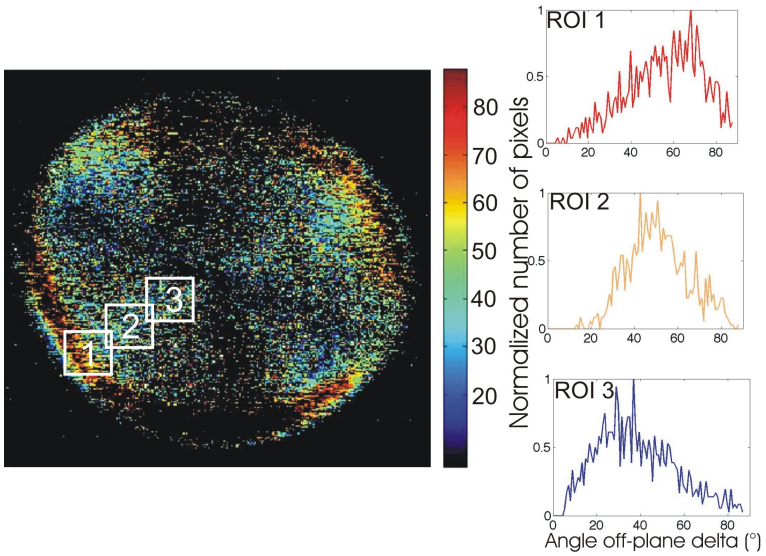

Fig. 5. The left image shows the distribution of the anisotropy parameter B in the equator of a starch granule. The three histogram for the angle δ on the right have been obtained from the three numbered regions of interest (ROI) shown in the left image.

Table 1. Comparative 3D-PSHG between two different imaging planes of a starch granule (n = 10)

	Off the equator				Equator			
	A	B	θ_e (°)	δ (°)	A	B	θ_e (°)	δ (°)
Peak	1.09	2.9	40.0	33.7	1.02	3.52	36.1	48.0
Δp	0.06	0.05	0.8	0.9	0.06	0.06	0.8	0.7
Width	0.53	1.22	6.8	38.7	0.53	1.18	5.4	39.2
Δw	0.02	0.03	0.1	0.6	0.02	0.01	0.1	0.7

#171632 - $15.00 USD Received 29 Jun 2012; rev. 8 Sep 2012; accepted 22 Sep 2012; published 28 Sep 2012

3.4. Hydration of starch: measuring the degree of amylopectin's organization

Recently, the width of the image histograms has been used to assign changes between normal and diseased collagen using the classical approach where all the molecules are assumed to be in plane (δ = 90°) [24]. Although in this PSHG study of pathological tissue the width of the image histograms was larger than the control (normal) case [24], no further structural elucidation was provided. Thus, information offered by the width of the image histograms still needs to be interpreted and to be correlated to the actual morphological characteristics of the sample. To address this issue, here we take advantage on the inherent property of starch granules to further organize upon hydration [23].

In this set of experiments we used the 40x, NA = 0.6 objective for excitation and a 40x NA = 0.95 for collection of the SHG signal. In order to better examine the effect of the tilted of the plane filaments, we retrieve the parameter B in the same wheat starch granules before (dried) and after hydration and we compare the pixels values histograms for the helical pitch angle θ_e (fixing δ = 90°) and angle δ (fixing d_{33}/d_{15} = 3.7). Hydration (instantaneous) was performed filling all the volume between the cover slips with distilled water. Since the values of the B parameter depends on the imaging planes, the PSHG measurement where carefully chosen to be performed in the plane where the recorded SHG signal was maximum (close to the equator of the granule) for both dried and hydrated starch. The use of water better matches the glass slides refractive index. Therefore, the light reaching the sample is expected to increase. In addition the molecules in the granule are further organized, improving the signal generation. These two effects are corroborated by our measurements, since upon hydration the first observed effect was an enhancement of almost a factor of three of the SHG signal. However, since the PSHG imaging technique is based on the SHG response on the excitation linear polarization, i.e., on the SHG signal modulation, this increase of the SHG signal intensity does not importantly affect the results.

In Fig. 6 we note that the center of the image histogram for the helical pitch angle is at θ_e = 37.8° in hydrated starch. This value is very close to the one obtained for dried starch (θ_e = 37.5°), indicating that under hydration the SHG active molecule (amylopectin) does not change. Although, the SHG source molecule (amylopectin) is further organized, forming lamellae [23], the experimentally retrieved helical pitch angle remains intact. This leads us to conclude that amylopectin molecule does not change structure under hydration. Nevertheless, the width of the image histogram (Fig. 6) for the B parameter, the pitch angle θ_e and the angle

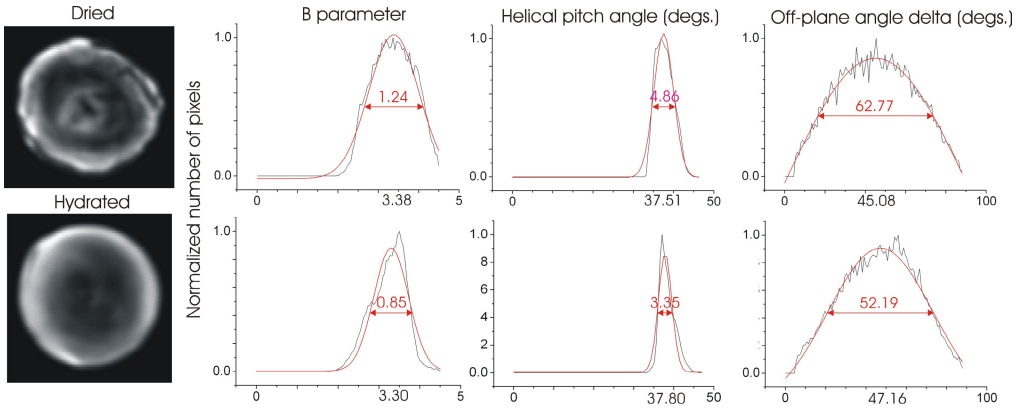

Fig. 6. Comparison between equatorial 2D and 3D-PSHG of the same dried and hydrated starch. The image histograms for the helical pitch are centered at $\theta_{e(dried)}$ = 37.5°and $\theta_{e(hydrated)}$ = 37.8° indicating that the helical pitch angle of amylopectin does not change under hydration. Under hydration starch is more organized and the width for the retrieved B parameter is ~33% narrower for the hydrated than the width of the less organized dried one. This is translated in a δ off-plane width ~17% narrower in hydrated starch.

#171632 - $15.00 USD Received 29 Jun 2012; rev. 8 Sep 2012; accepted 22 Sep 2012; published 28 Sep 2012

δ substantially changes upon hydration, resulting in a value ~32%, 31% and ~17% narrower than the width of the dried starch, respectively. The experiment was performed in 10 granules, resulting in a mean for the histogram width for the B parameter of 1.19 ± 0.08 and 0.88 ± 0.04 in dried and hydrated starch, respectively. Considering the fact that hydration increases the organization of amylopectin molecules, we conclude that the width of the image histograms for the *B* parameter is consequence of the number of molecules tilted off the plane. Therefore, the width of *B* or the angle δ provides a measurement of the degree of organization of the amylopectin molecules, in principle discharging any variation in the molecular structure as a source of the observed narrowing (the width in θ_e is an artifact caused by the existence of tilted-off molecules). From the above discussion we conclude that the organization of amylopectin caused by hydration is reflected in the width of the image histograms. The shorter the width is, the more organized the molecules in the sample are.

4. Conclusions

Polarization sensitive SHG imaging or PSHG offers additional information and means of contrast than intensity only SHG. In particular, it reflects a structurally dependent response of the experimentally retrieved $\chi^{(2)}$ elements ratio. In the present study we have examined the effect of the tilted-off the plane SHG active molecules to that polarization response. For that, we used a 3D PSHG model applied to starch granules. Starch granules possess a convenient radial architecture of the SHG active molecule, amylopectin. Then, by performing a PSHG measurement in different *z*-plane and different regions of interest we found differences in the image histograms. These differences are consistent with the existence of tilted off plane molecules and not with change in the amylopectin's helical pitch angle.

Then we performed starch hydration, which organizes the amylopectin molecules into a structure called crystalline lamellae. After performing PSHG we found that the width of the image histogram for the anisotropy parameter *B* was ~32% narrower in hydrated starch than in dried starch. Thus, the width of the image histogram of the anisotropy parameter (or alternatively the off-plane angle) can provide a measure of the degree of organization. The narower the width is, the more organized the amylopectin molecules in starch are. This result can be extrapolated to other SHG samples, attributing the effect of molecular organization to changes in the width of the PSHG image histograms.

Acknowledgments

This work is supported by the Generalitat de Catalunya (2009-SGR-159) and by the Spanish government (TEC2009-09698 and FIS2009-09928). Authors also acknowledge the Laser Lab Europe (optobio), the Photonics4Life network of excellence and the European Regional Development Fund. This research has been partially supported by Fundació Cellex Barcelona and has been conducted at the super resolution light nanoscopy facility at ICFO.

#171632 - $15.00 USD Received 29 Jun 2012; rev. 8 Sep 2012; accepted 22 Sep 2012; published 28 Sep 2012